HHS Public Access

Author manuscript

Stem Cells. Author manuscript; available in PMC 2017 February 01.

Published in final edited form as:

Stem Cells. 2016 February ; 34(2): 431–444. doi:10.1002/stem.2213.

Definitive hematopoiesis in the yolk sac emerges from Wnt-responsive hemogenic endothelium independently of circulation and arterial identity

Jenna M. Frame[1,2], **Katherine H. Fegan**[1], **Simon J. Conway**[3], **Kathleen E. McGrath**[1], and **James Palis**[1,*]

[1]Department of Pediatrics, Center for Pediatric Biomedical Research, University of Rochester Medical Center, Rochester, NY, USA

[2]Department of Pathology and Laboratory Medicine, University of Rochester Medical Center, Rochester, NY, USA

[3]Department of Pediatrics, Herman B. Wells Center for Pediatric Research, Indiana University School of Medicine, Indianapolis, IN, USA

Abstract

Adult-repopulating hematopoietic stem cells (HSCs) emerge in low numbers in the midgestation mouse embryo from a subset of arterial endothelium, through an endothelial-to-hematopoietic transition. HSC-producing arterial hemogenic endothelium relies on the establishment of embryonic blood flow and arterial identity, and requires β-catenin signaling. Specified prior to and during the formation of these initial HSCs are thousands of yolk sac-derived erythro-myeloid progenitors (EMPs). EMPs ensure embryonic survival prior to the establishment of a permanent hematopoietic system, and provide subsets of long-lived tissue macrophages. While an endothelial origin for these HSC-independent definitive progenitors is also accepted, the spatial location and temporal output of yolk sac hemogenic endothelium over developmental time remains undefined. We performed a spatiotemporal analysis of EMP emergence, and document the morphological steps of the endothelial-to-hematopoietic transition. Emergence of rounded EMPs from polygonal clusters of Kit^+ cells initiates prior to the establishment of arborized arterial and venous vasculature in the yolk sac. Interestingly, Kit^+ polygonal clusters are detected in both arterial and venous vessels after remodeling. To determine whether there are similar mechanisms regulating the specification of EMPs with other angiogenic signals regulating adult-repopulating HSCs, we investigated the role of embryonic blood flow and Wnt/β-catenin signaling during EMP emergence. In embryos lacking a functional circulation, rounded Kit^+ EMPs still fully emerge from unremodeled yolk sac vasculature. In contrast, canonical Wnt signaling appears to be a common mechanism regulating hematopoietic emergence from hemogenic endothelium. These

*Correspondence: James Palis, M.D., Center for Pediatric Biomedical Research, University of Rochester Medical Center, 601 Elmwood Ave., Box 703, Rochester, NY, 14642, Tel: 585-275-5098, Fax: 585-276-0232, James_Palis@urmc.rochester.edu.

Author Contributions: J.M.F. and K.E.M.: conception and design, collection and assembly of data, data analysis and interpretation, manuscript writing, and final approval of manuscript; K.H.F.: collection and assembly of data; S.J.C.: provision of study material; J.P.: conception and design, financial support, data analysis and interpretation, manuscript writing, and final approval of manuscript.

Disclosure of Potential Conflicts of Interest

The authors have no conflicts of interest.

data illustrate the heterogeneity in hematopoietic output and spatiotemporal regulation of primary embryonic hemogenic endothelium.

Graphical Abstract

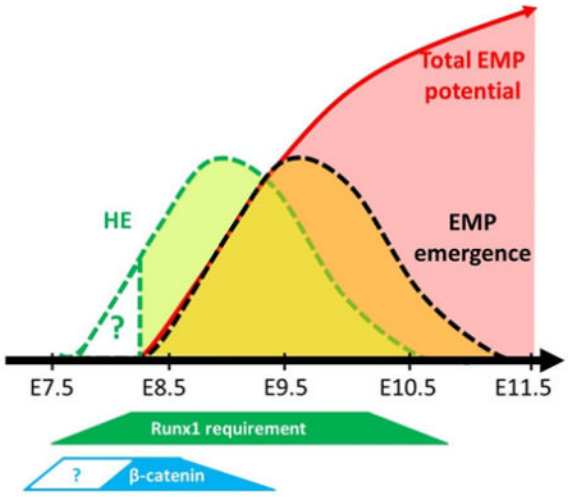

Keywords

Hematopoietic stem cells; Hematopoiesis; Hematopoietic progenitors; Vascular Development; Endothelial cell; Embryo; Hemangioblast

Introduction

The first hematopoietic stem cells (HSCs) in vertebrates arise from cells with arterial endothelial identity. These hemogenic endothelial cells, distinguished by expression of the critical hematopoietic transcription factor Runx1, reside in the aorta, umbilical artery, and vitelline artery of the midgestation murine embryo[1–6]. Hemogenic endothelium in these locations produces hematopoietic cell clusters that appear to form from the protrusion and proliferation of single or small numbers of hemogenic endothelial cells into the vascular lumen. Seminal live imaging experiments have captured the initial stages of the endothelial-to-hematopoietic transition in both zebrafish embryos and tissue sections of murine embryos[7–10], and fate-tracing experiments have established that hematopoietic cells arise from VE-Cadherin^{+} and Tie2^{+} populations[11, 12]. The spatiotemporal location of hemogenic endothelial cell clusters in the murine major arteries has been mapped[13, 14], and correlates with functional assays pinpointing HSC activity to the ventral aspect of the dorsal aorta[15]. Significantly, mapping HSC emergence to this specific embryonic location during a defined developmental time has facilitated the discovery of developmental regulators that influence the formation of hemogenic endothelium.

Signaling pathways regulating the specification of the aorta and hemogenic endothelium therein have been extensively studied. Functional arteries and veins must form prior to embryonic day (E)10 to allow blood flow and oxygenation of the growing murine

embryo[16, 17]. Thus, arterial specification precedes HSC emergence, and both require a well-defined signaling cascade. Hedgehog controls VEGF signaling, which regulates the Notch pathway, shown to be critical for both arterial specification[18] and Runx1 expression[19, 20]. In addition, nitric oxide signaling, which is controlled by blood flow, also influences Runx1 expression[21, 22]. Canonical Wnt signaling also regulates vascular remodeling, by increasing expression of Notch pathway components[23, 24]. Not surprisingly, canonical Wnt signaling was recently shown to regulate HSC formation in the aorta[25, 26]. Epistasis studies in developing zebrafish have further delineated the interplay between Wnt/β-catenin signaling, blood flow, and Notch signaling during HSC specification[21]. Consequently, arterial specification and HSC emergence from hemogenic endothelium appear tightly intertwined.

Despite this focus on HSC emergence, hematopoiesis has multiple developmental origins. Prior to HSC formation, two transient waves of hematopoiesis emerge in the yolk sac[27]. The first wave gives rise to progenitors as early as murine embryonic day (E)7.5 that produce primitive erythroblasts, megakaryocytes and macrophages[27, 28]. By E8.25, a second wave of erythro-myeloid progenitors (EMPs) begins to emerge in the yolk sac, and colonizes the fetal liver prior to HSCs[29]. While EMPs are transient, they serve as a critical source of fetal hematopoiesis before HSCs expand and differentiate[30], generating the first circulating definitive erythrocytes by E11.5[31]. Thus, EMPs have been categorized as "definitive" based on the original criteria used to distinguish the two initial sources of circulating erythroid cells in the mammalian embryo[29, 32]. Recent evidence also indicates that EMPs are a source of tissue-resident myeloid cell populations that persist into adulthood[33, 34].

The mechanisms regulating EMP emergence in the yolk sac are less defined. Like HSCs, EMPs rely on Runx1 for formation, and express endothelial markers, suggesting an endothelial ancestry[3, 4, 35–37]. However, EMPs arise during the remodeling of an initial plexus of yolk sac endothelium into arborized networks of arteries and veins[27, 38]. In addition, the persistence of EMP colony-forming activity in the absence of blood flow also suggests that EMPs do not require blood flow for specification[39]. Despite these differences, there are reports of Kit^+ or $CD41^+$ cell clusters within the yolk sac at early stages[40–42]. However, hematopoietic progenitors in the yolk sac increase through at least E10.5[27], and the temporal kinetics and spatial location of EMP production within the remodeled yolk sac vasculature throughout this time remains undefined. Here, we provide further histological evidence that EMPs emerge from hemogenic endothelium, and define the window of EMP production *in situ* by analyzing the morphology and numbers of emerging progenitors over developmental time. We also mapped the spatial distribution of emerging EMPs as an initial step toward understanding their regulation. Finally, we provide data supporting a common role for Wnt signaling in promoting hematopoietic emergence from hemogenic endothelium.

Materials and Methods

Mouse strains and tissue isolation

Outbred Swiss Webster mice (Taconic) were used for all experiments unless indicated. *Runx1*$^{+/-}$[4], *Ncx1*$^{+/-}$ [43], and *BAT-gal*[44] mice were previously described. *Cdh5-Cre* (B6;129-Tg(Cdh5-cre)1Spe/J)[45] and *Ctnnb1*$^{fl/fl}$ mice (B6.129-Ctnnb1^{tm2Kem}/KnwJ) [46] were purchased (Jackson Laboratory). Embryonic tissues and adult bone marrow were obtained as described[31, 47]. Mice were mated overnight, and the morning of plug detection was considered embryonic day (E)0.3[31]. For embryonic staging, somite pairs (sp) were enumerated when possible, and correlated with gestational age[48]. Embryonic tissues were dissociated at 37°C in 0.125% Collagenase (Stem Cell Technologies) in PB2[31] for 10 minutes, followed by trituration, a 1:1 dilution in PBS/1mM EDTA for 10 minutes, a second trituration, and 35μM filtration (Falcon). The University of Rochester Committee on Animal Resources approved all animal experiments.

Flow Cytometry and Imaging Flow Cytometry

Cells were labeled and sorted or analyzed using flow cytometry as described[37]. For imaging flow cytometry, cells were treated with or without 100 ng/mL Wnt3a (R&D Systems) for 2 hours, labeled with surface antibodies, fixed with 2% formaldehyde (Polysciences) for 10 minutes, permeabilized with 0.2% Triton-X-100 (Sigma) for 5 minutes, and stained with Alexa Fluor 488-anti-β-catenin (Cell Signaling Technology) for 1 hour, followed by a 10 min wash and addition of 1 μg/mL DAPI (Molecular Probes). The data were collected with an ImageStream^X, and analyzed using IDEAS 6.1 software (Amnis, Millipore). β-catenin nuclear signal was determined as the intensity of β-catenin staining within the Morphology Mask of DAPI signal using the feature (Intensity_Morphology(M07, DAPI)_Ch02/β-catenin). Assessment of apoptosis using imaging flow cytometry was based on nuclear fragmentation and cytoplasmic vesiculation[49].

In vitro culture

Sorted cells were cultured for 3 days in myeloid maturation media[50]. For OP9 co-cultures, groups of 3 anterior or posterior halves of E8.5 yolk sacs were dissociated, cultured on OP9 monolayers (ATCC) in 25cm^2 flasks and assayed for hematopoietic potential[51]. Kit$^+$ cells from adult marrow were used as controls. Yolk sac explants were cultured individually in StemSpan (Stem Cell Technologies) supplemented with 25 ng/mL Stem Cell Factor (Peprotech) with or without 100 ng/mL Wnt3a (R&D Systems). Methylcellulose colony-forming assays (CFCs) and high-proliferative potential CFC assays (HPP-CFC) were performed as previously described[52, 53]. Cultured cells were cytospun and Wright-Giemsa stained as described[54].

Whole-mount immunohistochemistry and X-Gal staining

Conceptuses were isolated in PB2 with intact yolk sacs, with one or two intentional tears to ensure efficient labeling and washing, rinsed in PBS, and fixed in 100% acetone at −20°C for 10 minutes, or 2% formaldehyde in PBS at 4°C for 1 hour. Staining was performed essentially as described[55] with primary antibodies for Kit and/or Flk1, CD31 or CD41 (all

from BD), VE-Cadherin (eBioscience), Runx1 (Abcam), Gp1bβ (Emfret), or Sox17 (R&D Systems), and species-specific secondary antibodies conjugated to Alexa Fluor 594, Alexa Fluor 647 (Life Technologies), and/or IRDye 800CW (LI-COR). If multiple rat primary antibodies were used, staining was performed sequentially. Specific labeling of each primary antibody was initially determined by comparison with no primary staining controls. Runx1 antibody was also confirmed to give no signal in *Runx1*$^{-/-}$ yolk sacs. At least four 20 minute washes were performed between antibody incubations. Yolk sacs were removed from the embryo proper after dehydration and flat-mounted on Bond-Rite slides (Richard-Allan Scientific) with ProLong Gold Antifade media (Molecular Probes). Kit^{+} clusters were analyzed in n=5 E8.5, n=8 E9.0, n=15 E9.5, n=26 E10-E11, n=7 E11.5, and n=6 E12.5-E13.5 wildtype yolk sacs (E12.5 and E13.5 not shown). For additional detection of β-galactosidase activity, conceptuses were fixed in 2% formaldehyde in PBS at 4°C for 1 hour, immunolabeled as above, avoiding Alexa Fluor 647 due to spectral overlap with precipitate[56], and subsequently stained with 5-Bromo-4-chloro-3-indolyl β-D-galactopyranoside (X-Gal) (Sigma) without further fixation[57].

Microscopy

Images were acquired with an ORCA-R2 digital camera (Hamamatsu) with an X-Cite series 120 illuminator (EXFO), or a Ds-Fli1 digital camera (Nikon) with NIS-Elements AR software on an Eclipse 80i microscope (Nikon) with 4x (Numerical Aperture (NA) 0.13), 10x (NA 0.3), 20x (NA 0.5), or 40x (NA 0.75) objectives. Hemoglobin autofluorescence at 515–555nm was used to identify primitive erythroblasts. Live images of megakaryocyte and macrophage cultures were captured with a Ds-Fli1 digital camera (Nikon) on an Eclipse TE2000-S microscope (Nikon) with a 20x objective (NA 0.45). Confocal images were acquired on a TCS SP5 microscope (Leica) with a 40x objective (NA 1.25). Images were processed for uniform brightness and contrast using NIS-Elements AR and/or Adobe Photoshop. Whole yolk sac images were merged from several 4x or 10x images with Adobe Photoshop.

Gene expression analysis

RNA was isolated as described[31]. cDNA was synthesized with iScript reagents (Bio-Rad) according to the manufacturer's instructions. Quantitative real-time PCR was performed on a CFX Connect (Bio-Rad) with Roche FastStart Universal SYBR Green mastermix (Roche) and analyzed as described[31]. Axin2 primer sequences were 5′-GGCTGCGCTTTGATAAGGTC and 5′-TGTGAGCCTCCTCTCTTTTACAG.

Results

Emerging EMPs progress from an endothelial to hematopoietic immunophenotype

Definitive hematopoietic potential in the E8.5 yolk sac resides in the Kit^{+}CD41^{+} population, and is associated with expression of endothelial markers[41, 58, 59]. Significant expression of the endothelial markers Flk1 and VE-Cadherin were detected on this population at E8.5 (Fig. 1A). By E9.5, endothelial marker co-expression was reduced on the Kit^{+}CD41^{+} fraction, while increases in the hematopoietic marker CD45 and the granulocyte-monocyte progenitor marker CD16/32 were observed in a majority of the population (Fig. 1A). This

shift in CD16/32 expression coincides with the reported shift of EMP colony-forming potential from both $Kit^+CD41^+CD16/32^+$ and $Kit^+CD41^+CD16/32^{neg}$ fractions of the E8.5 yolk sac, to reside almost exclusively in a now uniform $Kit^+CD41^+CD16/32^+$ fraction by E9.5 [37]. Consistent with an immunophenotypic shift, and not the loss of $Kit^+CD16/32^{neg}$ cells during this time, less than 1% of E8.5 Kit^+ cells exhibited morphological characteristics indicative of apoptosis using imaging flow cytometry (data not shown). Importantly, CD16/32 cell surface expression was also upregulated on E8.5 $Kit^+CD41^+CD16/32^{neg}$ cells cultured *in vitro* (Fig. 1B), indicating that the E8.5 $Kit^+CD41^+CD16/32^{neg}$ fraction matures into $Kit^+CD41^+CD16/32^+$ EMPs. Together, these data support the hypothesis that E8.5 EMPs undergo an endothelial-to-hematopoietic transition between E8.5 and E9.5.

Kit distinguishes Runx1-dependent EMPs from maturing hematopoietic lineages in the yolk sac

Previous studies have utilized CD41 or Kit to label emerging EMPs at E8.5 and E9.5[36, 40–42]. However, primitive erythroblasts, macrophages, and megakaryocytes reside in the yolk sac with nascent EMPs, and these populations may also express these markers during their maturation[27, 28, 60]. To identify the most accurate phenotypic marker to exclusively label EMPs throughout their emergence, the hematopoietic potential associated with each marker was evaluated. This analysis revealed a population of $CD41^{hi}Kit^{neg}$ cells that express high levels of the megakaryocyte-specific marker Gp1bβ (Fig. 1C, black), and formed proplatelets *in vitro* (Fig. 1D, ii). Though the majority of the Kit^+ fraction expresses CD16/32 and variable levels of CD45 (Fig. 1C, blue), there was also a population of $CD16/32^+Kit^{neg}$ cells that were also $CD45^{hi}$ (Fig. 1C, green) and generated macrophages in culture (Fig. 1D, iii). As a control, the purified $Kit^+CD41^+CD16/32^+$ EMP population (not shown) formed immature erythroblasts, megakaryocytes, macrophages, and granulocytes when cultured *in vitro* (Fig. 1D, i)[37]. These data indicate that CD41, and CD45 and CD16/32 are significantly expressed by differentiating megakaryocytes and macrophages, respectively, in the yolk sac.

Consistent with the required role for Runx1 in initiating the endothelial-to-hematopoietic transition[45], there was a lack of $Kit^+CD41^+CD16/32^+$ EMPs in *Runx1*$^{-/-}$ yolk sacs, as very few Kit^+ cells remained (Fig. 1C, blue). We also confirmed expression of *Runx1*, along with required transcriptional regulators *Gata2*, *Fli1*, and *Tal1*, in purified EMPs[61] (Fig. S1A). The $CD16/32^+Kit^{neg}$ macrophage population was also significantly depleted in *Runx1*$^{-/-}$ yolk sacs, while the $CD41^+Kit^{neg}$ megakaryocyte and $Ter119^+Kit^{neg}$ erythroblast populations remained, albeit with decreased expression of Gp1bβ and Ter119[62] (Fig. 1C, and data not shown). The persistence of these populations in *Runx1*$^{-/-}$ yolk sacs is in accordance with the initial derivation of megakaryocytes and macrophages from primitive hematopoietic progenitors[27, 28, 60].

As expected from the flow cytometry analysis, there was significant overlap in expression of Gp1bβ with $CD41^+$ cells at E9 by immunohistochemistry (Fig. 1E), suggesting megakaryocyte commitment in these cells. CD41 labeling was also not evident on all Kit^+ cells (Fig. 1F), which is consistent with lower expression of CD41 on EMPs compared to

maturing megakaryocytes (Fig. 1C), and Kit expression prior to CD41 at the hemogenic endothelial stage *in vitro*[63, 64]. Given these findings, we considered Kit to be the earliest and most specific marker of definitive hematopoietic commitment. We also confirmed the absence of Kit^+ cells in *Runx1*$^{-/-}$ yolk sacs by immunohistochemistry (Fig. S1B). Taken together, these data indicate that CD16/32, CD45, and CD41 do not exclusively label emerging EMPs. However, Kit unambigiously labels emerging hematopoietic progenitors in the yolk sac, just as was demonstrated for HSC clusters in the aorta[13].

Morphology of Kit^+ EMPs is consistent with an endothelial-to-hematopoietic transition

To visualize the morphological changes of emerging EMPs in the yolk sac, immunohistochemistry was performed for Kit, Runx1, and endothelial markers CD31, VE-Cadherin, and Flk1. At E8.5, a subset of $CD31^+$ cells with endothelial morphology expressed Runx1 and Kit (Fig 2A, arrows). Other $Runx1^+CD31^+Kit^+$ cells exhibited a more rounded morphology, indicating they are in the process of emerging, or have already emerged from the endothelial layer (Fig. 2A, arrowheads). $Kit^{lo}Runx1^+$ cells with endothelial morphology are present in rare numbers, suggesting this initial stage of the endothelial-to-hematopoietic transition is extremely transient (Fig. 2B). Moreover, the direct association of rare flattened $Kit^{lo}Runx1^+$ cells with Kit^+ rounded hematopoietic cells is consistent with a morphologic transition of flattened Kit^{lo} cells into Kit^+ rounded cells.

In contrast to the rare Kit^{lo} endothelium, Kit^+ cells exhibited two distinctive morphologies. While some were rounded with hematopoietic morphology (Fig. 2B and 2C), other Kit^+ cells demonstrated a polygonal morphology, and were present in clusters with angular cell-cell boundaries resembling those found between true endothelial cells (Fig. 2C, open arrows). Some polygonal Kit^+ clusters consisted of multiple layers of tightly associated polygonal cells reminiscent of murine HSC clusters observed protruding into the lumen of the major arteries[13]. Many Kit^+ cells within, or associated with, polygonal Kit^+ clusters appeared to be in the process of becoming rounded (Fig. 2C, closed arrows). Further assessment of clusters with confocal microscopy highlight this polygonal morphology, and reveal Kit signal in the same plane of focus as the $Flk1^+$ endothelium (Fig. 2D), suggesting that the polygonal Kit^+ cells are embedded in the vessel wall. Kit^+ clusters with both polygonal and rounded morphology were observed from E8.5 through E11, which is consistent with a continuous, yet heterogeneous emergence of EMPs via an endothelial-to-hematopoietic transition throughout this time frame (Fig. 2C). Interestingly, cluster sizes also appeared to get progressively larger over developmental time through E11 (Fig. 2C).

To quantify the temporal kinetics of EMP production, the frequency of emerging Kit^+ clusters was assessed. Clusters of 10–49 cells were most numerous at E9.5 (20–23sp), and gradually declined over developmental time (Fig. 3A). There was also a trend toward an increase in the number of large clusters (≥50 cells) at E10.5-E11. After E11.5, only rare clusters were observed (data not shown), signifying the exhaustion of $Kit^{lo}Runx1^+$ hemogenic endothelial potential in the yolk sac. These observations of Kit^+ clusters as late as E11.5 indicate that EMP emergence in the yolk sac temporally overlaps in part with HSC emergence in the major arteries[13]. Importantly, this exhaustion of EMP production at E11.5 does not signify a loss of EMPs, as flow cytometry analyses identified significant

numbers of Kit$^+$ cells present in the yolk sac through E12, presumably in the bloodstream en route to the fetal liver[37]. This analysis also confirmed that the majority of Kit$^+$ cells in the yolk sac through E12 are Kit$^+$CD41$^+$CD16/32$^+$ EMPs (Fig. 3B). Together, these data indicate that EMPs are produced during a defined developmental window, but that they persist as a robust progenitor population in the embryo through at least E12.

Yolk sac hemogenic endothelium is not confined to arterial vasculature

To gain additional insight into the regulation of yolk sac hemogenic endothelial specification with respect to the total pool of endothelium, the spatial location of emerging EMPs was investigated over developmental time. At the onset of hemato-vascular development, a pool of CD31$^+$ endothelium envelops primitive erythropoietic progenitors, forming “blood islands” that are restricted to the proximal region of the yolk sac[65]. By 2sp, or early E8.25, CD31$^+$ endothelium extends distally to form a vascular plexus throughout the yolk sac[55, 66]. Kit$^+$ EMP clusters were preferentially located in the proximal region of the yolk sac vasculature, and were interspersed between the primitive erythroblasts (Fig. 4A, Fig. S2A–C). This preference for EMP clusters in the proximal yolk sac was preserved at E9 (Fig. 4B), although some clusters were observed in the distal half of the yolk sac closer to the vitelline vessels after vascular remodeling (Fig. 4C). These findings indicate that EMP emergence occurs along a proximal-distal gradient in the yolk sac.

At E8.5, Ephrinb2 expression indicates that arterial identity is specified in the posterior vasculature of the yolk sac prior to vascular remodeling[67]. Interestingly, we observed Kit$^+$ clusters in both the anterior and posterior regions of the E8.5 yolk sac (Fig.4A, Fig. S2A–C). Consistent with a lack of anterior/posterior asymmetry of clusters at E8.5, Kit$^+$ EMP clusters at E9 and E9.5 were detected in both the arterial and venous vasculature after remodeling of the yolk sac commenced[68] (Fig. 4B and 4C). We also confirmed the arterial identity of the vasculature branching from the vitelline artery with Sox17 labeling, and found evidence of rare Runx1$^+$Sox17$^+$ cells (Fig. S3)[24, 69]. Together, these results indicate that EMPs can emerge from arterial vasculature, but suggests they do not require arterial identity for specification.

We next tested the capacity of the venous and arterial regions of the yolk sac to generate definitive hematopoietic progenitors. E8.5 yolk sacs were bisected into anterior and posterior halves, dissociated, and co-cultured with OP9 stroma[51]. Cultures of both anterior and posterior yolk sacs produced definitive GR-1$^+$ granulocytes (Fig. 4D), confirming the emergence of functional EMPs from both venous and arterial vasculature. Though EMPs constitute the majority of definitive hematopoietic potential in the yolk sac, it was recently established that there are also rare Kit$^+$ lymphoid progenitors in the yolk sac[51, 70, 71], that are separate from Kit$^+$CD41$^+$CD16/32$^+$ EMPs[37]. Since lymphoid potential has also been associated with the emergence of HSCs in arterial vasculature, we also tested for B-lymphoid potential. Interestingly, a low frequency of B cells also emerged in both anterior and posterior regions of the yolk sac, suggesting that B-lymphoid potential in the yolk sac is not dependent on arterial identity (Fig. 4D). Taken together, these results suggest that

hematopoietic specification in the yolk sac, including primitive, EMP and B-lymphoid potential, is regulated by a proximal-distal gradient rather than arterial/venous identity.

EMPs emerge from unremodeled vasculature in the absence of circulation

Hemodynamic forces are required for both HSC emergence and angiogenesis, and in the yolk sac, shear forces capable of modulating endothelial behavior *in vitro* have been detected as early as E8.5[22, 72, 73]. Therefore, to address whether EMP emergence *in situ* was also altered in the absence of blood flow, the location and morphology of Kit^+ clusters was analyzed in the yolk sac of circulation-deficient $Ncx1^{-/-}$ embryos. While previous analyses demonstrated presence of definitive hematopoietic colony-forming activity in $Ncx1^{-/-}$ yolk sacs, these studies were performed on enzymatically dissociated yolk sacs, and therefore could not assess whether fully rounded EMPs were able to emerge from the endothelial layer in the absence of flow[39, 74]. Interestingly, in contrast to the reliance of aortic hemogenic endothelium on blood flow, normal EMP cluster morphology and location was observed in $Ncx1^{-/-}$ yolk sacs, including the presence of Kit^+ rounded EMPs (Fig. 5A–B), and $Runx1^+$ hemogenic endothelium (Fig. 5C).

EMPs emerge in larger and smaller vessels after vascular remodeling of the yolk sac

HSC-producing hemogenic endothelium is located exclusively in the largest arterial vessels of the embryo, including the portion of the vitelline artery closer to the embryo proper than to the yolk sac[75]. We therefore asked whether the presence of hemogenic endothelium was preferentially associated with large vessels of the yolk sac after vascular remodeling. Despite the independence of EMPs from arterial identity and blood flow, flattened Kit^{lo} cells and polygonal Kit^+ cells were identified not only in smaller vessels, but also in larger vessels of the yolk sac vascular plexus after remodeling at E9.5-E10 (Fig. 5D–F). These findings further highlight the heterogeneity in the distribution of hemogenic endothelium within the remodeling vasculature of the yolk sac.

Canonical Wnt signaling regulates EMP emergence

Since β-catenin is an important regulator of HSC-producing hemogenic endothelium in both mouse and zebrafish[25, 26, 76], we next asked whether Wnt signaling regulates EMP specification. Treatment of intact yolk sacs with the canonical ligand Wnt3a for 48 hours increased the total pool of definitive hematopoietic progenitors, as well as the highly proliferative HPP-CFC (Fig. 6A). This increase in EMPs was not likely due to self-renewal, as treatment of isolated EMPs with Wnt3a *in vitro* did not lead to an increase in CFC numbers (Fig. 6B). These findings suggest that Wnt3a regulates EMP formation at or prior to the hemogenic endothelial precursor stage. Consistent with this hypothesis, Wnt3a treatment increased β-catenin staining in the nuclear area of E9.5 Kit^+AA4.1/VE-$Cadherin^+$ hemogenic endothelium assayed by imaging flow cytometry (Fig. 6C). Additionally, treatment of the E9.5 AA4.1/VE-$Cadherin^+$$CD16/32^{neg}$ fraction with Wnt3a increased expression of the β-catenin target gene *Axin2* (Fig. 6D). Together, these data suggest that hemogenic endothelial cells in the yolk sac are responsive to canonical Wnt signaling.

To investigate endogenous β-catenin activity, we analyzed the yolk sacs of β-catenin reporter (*BAT-gal*) mice. Immunohistochemical analysis of X-Gal stained yolk sacs revealed

β-galactosidase (β-gal) activity in endothelial cells (Fig. S4A)[24, 77, 78], and a rare subset of β-gal$^+$Runx1$^+$VE-Cadherin$^+$ cells, suggesting that some Wnt-responsive endothelial cells are hemogenic (Fig. 6E). Consistent with a transient role for Wnt signaling during hematopoietic specification [25, 76], the majority of Runx1$^+$ cells were negative for β-galactosidase activity (Fig. 6E, Fig. S4), and assessment at E9.5 demonstrated a marked reduction in Wnt/β-catenin activity (not shown).

To address the function of Wnt signaling in EMP emergence *in vivo*, β-catenin was ablated in a hemato-endothelial specific manner in *Cdh5-Cre; ctnnb1$^{fl/fl}$* embryos (*β-catenin^{cKO}*)[45, 46]. Significantly, hematopoietic progenitor numbers in E9.5-E10.5 *β-catenin^{cKO}* yolk sacs were reduced compared with littermates lacking *Cdh5-Cre* (Fig. 6F). Together, these data support the concept that β-catenin intrinsically promotes the emergence of definitive hematopoietic potential in yolk sac hemogenic endothelium.

Overall, our findings suggest that EMPs are produced from a broad temporal wave of hemogenic endothelium that is responsive to Wnt/β-catenin signaling during a specific developmental window (Fig. 7A). This wave of hemogenic endothelium in the yolk sac generates Kit$^+$ EMP clusters that continue to emerge as late as E11.5, temporally overlapping with HSC emergence (Fig. 7A, orange; Fig. 7B). Large numbers of circulating EMPs are present in the E11.5-E12 mouse conceptus[37], which seed the fetal liver and ultimately perform their hematopoietic function (Fig. 7A, red curve).

Discussion

Definitive hematopoiesis in vertebrates is initiated via an endothelial-to-hematopoietic transition that occurs at precise developmental times in distinct embryonic vasculatures. Interestingly, this process gives rise to HSCs and progenitors with fundamentally distinct self-renewal capabilities and lineage potential. Regulation of this process has primarily been studied in the aorta, where HSCs are derived from arterial hemogenic endothelium in a blood flow and β-catenin-dependent manner. However, the spatiotemporal localization and regulation of hemogenic endothelium in the yolk sac remain unclear. Deciphering the origin and regulation of the multiple waves of embryonic hematopoiesis *in vivo* are necessary steps to better direct hematopoietic lineage and self-renewal potential *in vitro*, as it remains difficult to distinguish the identity of definitive hematopoietic cells derived from the *in vitro* differentiation of embryonic stem cell and induced pluripotent stem cell cultures. Here we provide further histological evidence that EMPs, like HSCs, arise from hemogenic endothelium, and reveal important mechanistic differences governing their emergence.

The expression of endothelial markers, combined with the dependence of definitive hematopoietic progenitors on Runx1, has implicated that EMPs also emerge through an endothelial-to-hematopoietic transition. We have determined that emerging Kit$^+$CD41$^+$ EMPs shift from an endothelial to hematopoietic immunophenotype when cultured *in vitro*. The paucity of other hematopoietic markers on nascent EMPs, and the lack of specificity of CD41, CD16/32, and CD45 for EMPs, indicates that Kit serves as the best marker to distinguish emerging EMPs from maturing megakaryocytes and macrophages in the yolk sac. Consistent with this specificity of Kit expression for EMPs, we confirmed the complete

lack of all Kit$^+$ cells and immunophenotypic EMPs in *Runx1*$^{-/-}$ yolk sacs. While it remains possible that a small subset of Kit$^+$ cells detected in our studies are rare lympho-myeloid progenitors[71], the robust numbers of Kit$^+$ cell clusters observed (Fig. 3A) support the conclusion that EMPs are derived from hemogenic endothelium.

The endothelial-to-hematopoietic transition in the yolk sac likely initiates with a Kit^{lo}Runx1$^+$ hemogenic endothelial population (Fig. 2A–B, Fig. 5F). The relative rarity of these cells suggests that this Kit^{lo}Runx1$^+$ endothelial stage is especially transient, and that the subsequent morphogenesis of polygonal Kit$^+$ clusters is a rate-limiting step for hematopoietic emergence. The persistence of these putative hemogenic endothelial cells at E10 is temporally consistent with previous studies suggesting an EMP requirement for Runx1 through E10.5[79]. In addition, the presence and abundance of cells within the polygonal Kit$^+$ clusters by E9.5 also strongly suggests they are still emerging from vasculature close to or in their observed location. Although circulation initiates at E8.25, almost all EMP activity remains in the yolk sac through E9.5[66], indicating that EMP clusters remain associated with the endothelial wall and are physically unable to circulate until later stages.

Primitive hematopoiesis initiates by E7.5 and produces hundreds of primitive erythroid progenitors in the blood island region of the yolk sac by E8.5, a time when the first few EMPs are detected[27, 28]. The dissimilarities in lineage potential and Runx1 requirement of primitive and definitive hematopoiesis raised the possibility that hemogenic endothelium might emerge spatially distinct from primitive hematopoiesis. However, we observed clusters of Kit$^+$ cells specifically dispersed within the blood islands, consistent with nascent derivation of both primitive and EMP-definitive hematopoiesis from common precursors. *In vitro* studies have revealed a population of hemangioblasts, which harbor primitive and definitive hematopoietic potential in addition to endothelial and smooth muscle potential, that emerge in the primitive streak during gastrulation[80]. Our findings that hemogenic endothelial clusters are initially localized in the proximal region of the yolk sac is consistent with, but does not prove, a common source of primitive and definitive hematopoietic potential[63, 80–82]. At later stages, we detected hemogenic endothelium in the distal yolk sac. Whether this relatively distal hemogenic endothelium we detected migrates from the proximal region during vascular remodeling and growth of the yolk sac[83], or relies on flow for hematopoietic commitment, is not discernable from these studies. However, the former hypothesis is supported by the normal numbers of EMPs that arise in circulation-deficient yolk sacs[39].

Together with the identification of rounded Kit$^+$ EMPs in the circulation-deficient yolk sac, our observations that EMPs emerge from the vascular plexus in anterior and posterior regions of the yolk sac, and arterial and venous vasculature after remodeling, suggests that they do not rely on arterial signals. This concept is also supported by the independence of endogenous EMP emergence on Notch1, a key mediator of arterial specification[84–86]. Interestingly, EMPs do arise in arterial regions of the yolk sac after remodeling, in agreement with at least some EMPs arising from a Sox17$^+$ population[87]. Taken together, these findings implicate a putative proximal-derived signal, rather than a posterior/arterial signal, in the regulation of yolk sac hematopoiesis.

Canonical Wnt signaling is active in the proximal yolk sac, and plays a role in murine primitive hematopoietic specification[88]. We observed canonical Wnt signaling in *BAT-gal* yolk sacs at E8.25-E8.5 (Fig. S4), when the first EMPs begin to emerge. Consistent with a role for β-catenin in the regulation of hemogenic endothelium[25, 76], we observed rare β-gal^{+}Runx1^{+} endothelial cells (Fig. 6E). Furthermore, loss of β-catenin initiated at the endothelial stage decreased numbers of functional EMPs, while *in vitro* Wnt3a treatment of phenotypically mature EMPs did not affect progenitor numbers. In the zebrafish aorta, the inductive effects of β-catenin on HSC emergence are blocked by nitric oxide synthase inhibition, suggesting that the effects of β-catenin on HSC emergence are mediated solely through blood flow[21]. Similarly, Notch signaling is downstream of β-catenin in the aorta[21]. Given the independence of EMP emergence both on blood flow and Notch signaling, it appears that Runx1 expression and commitment to hemogenic endothelium is alternatively regulated in the yolk sac, despite the common expression of other critical transcriptional regulators in EMPs (Fig. S1A). However, the conserved role of Wnt signaling in yolk sac hemogenic endothelium suggests an important role in regulating the endothelial-to-hematopoietic transition, rather than long-term hematopoietic potential.

Conclusion

Our findings provide evidence that EMPs emerge in both the presumptive venous (anterior) and arterial (posterior) vessels of the yolk sac from E8.25-E11 via a Runx1-dependent process of endothelial-to-hematopoietic transition (Fig. 7B). Despite the concurrent onset of EMP-derived hematopoiesis and angiogenesis, both arterial identity and embryonic blood flow are dispensable for EMP emergence. In contrast, EMP-producing hemogenic endothelium is specifically located in the proximal yolk sac, and is responsive to canonical Wnt signaling. Together, our results highlight key differences in the spatiotemporal and mechanistic control of hematopoietic specification in the mammalian conceptus.

Supplementary Material

Refer to Web version on PubMed Central for supplementary material.

Acknowledgments

We thank Dr. Michael Nemeth for helpful discussions, and Dr. Paul Kingsley, Leah Vit, Seana Catherman, Dr. Yu-Shan Huang, Anne Koniski, and the University of Rochester Flow Cytometry Core Facility for technical expertise and assistance. We thank Dr. Kate Ackerman and Nicole Paris for *BAT-gal* mice, and Dr. James Downing for *Runx1*$^{+/-}$ mice. This work was supported by the National Institutes of Health (R01-DK079361 to J.P.), a New York Stem Cell Science Fellowship (J.M.F.), and the Michael Napoleone Foundation.

References

1. Muller AM, Medvinsky A, Strouboulis J, et al. Development of hematopoietic stem cell activity in the mouse embryo. Immunity. 1994; 1:291–301. [PubMed: 7889417]
2. Bruijn MFTR, de Speck NA, Peeters MCE, et al. Definitive hematopoietic stem cells first develop within the major arterial regions of the mouse embryo. EMBO J. 2000; 19(11):2465–2474. [PubMed: 10835345]
3. Wang Q, Stacy T, Binder M, et al. Disruption of the Cbfa2 gene causes necrosis and hemorrhaging in the central nervous system and blocks definitive hematopoiesis. Proc Natl Acad Sci. 1996; 93(8): 3444–3449. [PubMed: 8622955]

4. Okuda T, Deursen J, van Hiebert SW, et al. AML1, the target of multiple chromosomal translocations in human leukemia, is essential for normal fetal liver hematopoiesis. Cell. 1996; 84:321–330. [PubMed: 8565077]
5. North T, Gu TL, Stacy T, et al. Cbfa2 is required for the formation of intra-aortic hematopoietic clusters. Development. 1999; 126(11):2563–2575. [PubMed: 10226014]
6. Kumaravelu P, Hook L, Morrison AM, et al. Quantitative developmental anatomy of definitive haematopoietic stem cells/long-term repopulating units (HSC/RUs): role of the aorta-gonad-mesonephros (AGM) region and the yolk sac in colonisation of the mouse embryonic liver. Development. 2002; 129(21):4891–4899. [PubMed: 12397098]
7. Boisset J-C, van Cappellen W, Andrieu-Soler C, et al. In vivo imaging of haematopoietic cells emerging from the mouse aortic endothelium. Nature. 2010; 464(7285):116–120. [PubMed: 20154729]
8. Bertrand JY, Chi NC, Santoso B, et al. Haematopoietic stem cells derive directly from aortic endothelium during development. Nature. 2010; 464(7285):108–111. [PubMed: 20154733]
9. Kissa K, Herbomel P. Blood stem cells emerge from aortic endothelium by a novel type of cell transition. Nature. 2010; 464(7285):112–115. [PubMed: 20154732]
10. Lam EYN, Hall CJ, Crosier PS, et al. Live imaging of Runx1 expression in the dorsal aorta tracks the emergence of blood progenitors from endothelial cells. Blood. 2010; 116(6):909–914. [PubMed: 20453160]
11. Li Z, Chen MJ, Stacy T, et al. Runx1 function in hematopoiesis is required in cells that express Tek. Blood. 2006; 107(1):106–110. [PubMed: 16174759]
12. Zovein AC, Hofmann JJ, Lynch M, et al. Fate Tracing Reveals the Endothelial Origin of Hematopoietic Stem Cells. Cell Stem Cell. 2008; 3(6):625–636. [PubMed: 19041779]
13. Yokomizo T, Dzierzak E. Three-dimensional cartography of hematopoietic clusters in the vasculature of whole mouse embryos. Development. 2010; 137(21):3651–3661. [PubMed: 20876651]
14. Yokomizo T, Ng CEL, Osato M, et al. Three-dimensional imaging of whole midgestation murine embryos shows an intravascular localization for all hematopoietic clusters. Blood. 2011; 117(23): 6132–6134. [PubMed: 21505195]
15. Taoudi S, Medvinsky A. Functional identification of the hematopoietic stem cell niche in the ventral domain of the embryonic dorsal aorta. Proc Natl Acad Sci USA. 2007; 104:9399–9403. [PubMed: 17517650]
16. Copp AJ. Death before birth: clues from gene knockouts and mutations. Trends Genet. 1995; 11(3):87–93. [PubMed: 7732578]
17. Coultas L, Chawengsaksophak K, Rossant J. Endothelial cells and VEGF in vascular development. Nature. 2005; 438(7070):937–945. [PubMed: 16355211]
18. Swift MR, Weinstein BM. Arterial-venous specification during development. Circ Res. 2009; 104(5):576–588. [PubMed: 19286613]
19. Burns CE, Traver D, Mayhall E, et al. Hematopoietic stem cell fate is established by the Notch-Runx pathway. Genes Dev. 2005; 19:2331–2342. [PubMed: 16166372]
20. Robert-MorenoÀ Espinosa L, de la Pompa JL, et al. RBPjκ-dependent Notch function regulates Gata2 and is essential for the formation of intra-embryonic hematopoietic cells. Development. 2005; 132(5):1117–1126. [PubMed: 15689374]
21. North TE, Goessling W, Peeters M, et al. Hematopoietic Stem Cell Development Is Dependent on Blood Flow. Cell. 2009; 137(4):736–748. [PubMed: 19450519]
22. Adamo L, Naveiras O, Wenzel PL, et al. Biomechanical forces promote embryonic haematopoiesis. Nature. 2009; 459(7250):1131–1135. [PubMed: 19440194]
23. Dejana E. The Role of Wnt Signaling in Physiological and Pathological Angiogenesis. Circ Res. 2010; 107(8):943–952. [PubMed: 20947863]
24. Corada M, Orsenigo F, Morini MF, et al. Sox17 is indispensable for acquisition and maintenance of arterial identity. Nat Commun. 2013; 4:2609. [PubMed: 24153254]
25. Ruiz-Herguido C, Guiu J, D'Altri T, et al. Hematopoietic stem cell development requires transient Wnt/β-catenin activity. J Exp Med. 2012; 209(8):1457–1468. [PubMed: 22802352]

26. Goessling W, North TE, Loewer S, et al. Genetic Interaction of PGE2 and Wnt Signaling Regulates Developmental Specification of Stem Cells and Regeneration. Cell. 2009; 136(6):1136–1147. [PubMed: 19303855]
27. Palis J, Robertson S, Kennedy M, et al. Development of erythroid and myeloid progenitors in the yolk sac and embryo proper of the mouse. Development. 1999; 126(22):5073–5084. [PubMed: 10529424]
28. Tober J, Koniski A, McGrath KE, et al. The megakaryocyte lineage originates from hemangioblast precursors and is an integral component both of primitive and of definitive hematopoiesis. Blood. 2007; 109(4):1433–1441. [PubMed: 17062726]
29. Frame JM, McGrath KE, Palis J. Erythro-myeloid progenitors: "Definitive" hematopoiesis in the conceptus prior to the emergence of hematopoietic stem cells. Blood Cells Mol Dis. 2013; 51(4): 220–225. [PubMed: 24095199]
30. Chen MJ, Li Y, De Obaldia ME, et al. Erythroid/Myeloid Progenitors and Hematopoietic Stem Cells Originate from Distinct Populations of Endothelial Cells. Cell Stem Cell. 2011; 9(6):541–552. [PubMed: 22136929]
31. McGrath KE, Frame JM, Fromm GJ, et al. A transient definitive erythroid lineage with unique regulation of the β-globin locus in the mammalian embryo. Blood. 2011; 117(17):4600–4608. [PubMed: 21378272]
32. Maximov A. Investigations of blood and connective tissue 1. The earliest stages of development of blood and tissue cells in the mammalian embryo until the beginning of the hematopoiesis in the liver [in German]. Arch Mikroskop Anat. 1909; 73:444–561.
33. Gomez Perdiguero E, Klapproth K, Schulz C, et al. Tissue-resident macrophages originate from yolk-sac-derived erythro-myeloid progenitors. Nature. 2015; 518(7540):547–551. [PubMed: 25470051]
34. Hoeffel G, Chen J, Lavin Y, et al. C-Myb+ Erythro-Myeloid Progenitor-Derived Fetal Monocytes Give Rise to Adult Tissue-Resident Macrophages. Immunity. 2015; 42(4):665–678. [PubMed: 25902481]
35. Nishikawa S-I, Nishikawa S, Kawamoto H, et al. In Vitro Generation of Lymphohematopoietic Cells from Endothelial Cells Purified from Murine Embryos. Immunity. 1998; 8(6):761–769. [PubMed: 9655490]
36. Goldie LC, Lucitti JL, Dickinson ME, et al. Cell signaling directing the formation and function of hemogenic endothelium during murine embryogenesis. Blood. 2008; 112(8):3194–3204. [PubMed: 18684862]
37. McGrath KE, Frame JM, Fegan KH, et al. Distinct Sources of Hematopoietic Progenitors Emerge before HSCs and Provide Functional Blood Cells in the Mammalian Embryo. Cell Rep. 2015; 11(12):1892–1904. [PubMed: 26095363]
38. Marcelo KL, Goldie LC, Hirschi KK. Regulation of Endothelial Cell Differentiation and Specification. Circ Res. 2013; 112(9):1272–1287. [PubMed: 23620236]
39. Lux CT, Yoshimoto M, McGrath K, et al. All primitive and definitive hematopoietic progenitor cells emerging before E10 in the mouse embryo are products of the yolk sac. Blood. 2008; 111(7): 3435–3438. [PubMed: 17932251]
40. Yokomizo T, Ogawa M, Osato M, et al. Requirement of Runx1/AML1/PEBP2αB for the generation of haematopoietic cells from endothelial cells. Genes Cells. 2001; 6(1):13–23. [PubMed: 11168593]
41. Ferkowicz MJ, Starr M, Xie X, et al. CD41 expression defines the onset of primitive and definitive hematopoiesis in the murine embryo. Development. 2003; 130(18):4393–4403. [PubMed: 12900455]
42. Li W, Ferkowicz MJ, Johnson SA, et al. Endothelial Cells in the Early Murine Yolk Sac Give Rise to CD41-expressing Hematopoietic Cells. Stem Cells Dev. 2005; 14(1):44–54. [PubMed: 15725743]
43. Koushik SV, Wang J, Rogers R, et al. Targeted inactivation of the sodium-calcium exchanger (Ncx1) results in the lack of a heartbeat and abnormal myofibrillar organization. FASEB J. 2001; 15(7):1209–1211. [PubMed: 11344090]

44. Maretto S, Cordenonsi M, Dupont S, et al. Mapping Wnt/-catenin signaling during mouse development and in colorectal tumors. Proc Natl Acad Sci. 2003; 100(6):3299–3304. [PubMed: 12626757]
45. Chen MJ, Yokomizo T, Zeigler BM, et al. Runx1 is required for the endothelial to haematopoietic cell transition but not thereafter. Nature. 2009; 457(7231):887–891. [PubMed: 19129762]
46. Brault V, Moore R, Kutsch S, et al. Inactivation of the (β)-catenin gene by Wnt1-Cre-mediated deletion results in dramatic brain malformation and failure of craniofacial development. Development. 2001; 128(8):1253–1264. [PubMed: 11262227]
47. Peslak SA, Wenger J, Bemis JC, et al. Sublethal radiation injury uncovers a functional transition during erythroid maturation. Exp Hematol. 2011; 39(4):434–445. [PubMed: 21291953]
48. Tam PPL. The control of somitogenesis in mouse embryos. J Embryol Exp Morphol. 1981; 65(Supplement):103–128. [PubMed: 6801176]
49. Henery S, George T, Hall B, et al. Quantitative image based apoptotic index measurement using multispectral imaging flow cytometry: a comparison with standard photometric methods. Apoptosis. 2008; 13(8):1054–1063. [PubMed: 18543109]
50. Arinobu Y, Iwasaki H, Gurish MF, et al. Developmental checkpoints of the basophil/mast cell lineages in adult murine hematopoiesis. Proc Natl Acad Sci USA. 2005; 102(50):18105–18110. [PubMed: 16330751]
51. Yoshimoto M, Montecino-Rodriguez E, Ferkowicz MJ, et al. Embryonic day 9 yolk sac and intra-embryonic hemogenic endothelium independently generate a B-1 and marginal zone progenitor lacking B-2 potential. Proc Natl Acad Sci. 2011; 108(4):1468–1473. [PubMed: 21209332]
52. Palis J, Chan RJ, Koniski A, et al. Spatial and temporal emergence of high proliferative potential hematopoietic precursors during murine embryogenesis. Proc Natl Acad Sci. 2001; 98(8):4528–4533. [PubMed: 11296291]
53. Palis J, Koniski A. Analysis of hematopoietic progenitors in the mouse embryo. Methods Mol Med. 2005; 105:289–302. [PubMed: 15492402]
54. Kingsley PD, Malik J, Fantauzzo KA, et al. Yolk sac-derived primitive erythroblasts enucleate during mammalian embryogenesis. Blood. 2004; 104(1):19–25. [PubMed: 15031208]
55. Ferkowicz MJ, Yoder MC. Whole embryo imaging of hematopoietic cell emergence and migration. Methods Mol Biol. 2011; 750:143–155. [PubMed: 21618089]
56. Levitsky KL, Toledo-Aral JJ, López-Barneo J, et al. Direct confocal acquisition of fluorescence from X-gal staining on thick tissue sections. Sci Rep. 2013; 3:2937. [PubMed: 24121824]
57. Pereira, FA. Whole-Mount Histochemical Detection of β-Galactosidase Activity. In: Ausubel, FM.; Brent, R.; Kingston, RE., et al., editors. Current Protocols in Molecular Biology. Hoboken, NJ, USA: John Wiley & Sons, Inc; 2001. Available at http://doi.wiley.com/10.1002/0471142727.mb1414s50
58. Kabrun N, Buhring HJ, Choi K, et al. Flk-1 expression defines a population of early embryonic hematopoietic precursors. Development. 1997; 124(10):2039–2048. [PubMed: 9169850]
59. Borges L, Iacovino M, Koyano-Nakagawa N, et al. Expression levels of endoglin distinctively identify hematopoietic and endothelial progeny at different stages of yolk sac hematopoiesis. STEM CELLS. 2013; 31(9):1893–1901. [PubMed: 23712751]
60. Potts KS, Sargeant TJ, Markham JF, et al. A lineage of diploid platelet-forming cells precedes polyploid megakaryocyte formation in the mouse embryo. Blood. 2014; 124(17):2725–2729. [PubMed: 25079356]
61. Pimanda JE, Ottersbach K, Knezevic K, et al. Gata2, Fli1, and Scl form a recursively wired gene-regulatory circuit during early hematopoietic development. Proc Natl Acad Sci. 2007; 104(45):17692–17697. [PubMed: 17962413]
62. Yokomizo T, Hasegawa K, Ishitobi H, et al. Runx1 is involved in primitive erythropoiesis in the mouse. Blood. 2008; 111(8):4075–4080. [PubMed: 18250229]
63. Lancrin C, Sroczynska P, Stephenson C, et al. The haemangioblast generates haematopoietic cells through a haemogenic endothelium stage. Nature. 2009; 457(7231):892–895. [PubMed: 19182774]
64. Eilken HM, Nishikawa S-I, Schroeder T. Continuous single-cell imaging of blood generation from haemogenic endothelium. Nature. 2009; 457(7231):896–900. [PubMed: 19212410]

65. Ferkowicz MJ, Yoder MC. Blood island formation: longstanding observations and modern interpretations. Exp Hematol. 2005; 33:1041–1047. [PubMed: 16140152]
66. McGrath KE, Koniski AD, Malik J, et al. Circulation is established in a stepwise pattern in the mammalian embryo. Blood. 2003; 101(5):1669–1675. [PubMed: 12406884]
67. Wang HU, Chen Z-F, Anderson DJ. Molecular Distinction and Angiogenic Interaction between Embryonic Arteries and Veins Revealed by ephrin-B2 and Its Receptor Eph-B4. Cell. 1998; 93(5): 741–753. [PubMed: 9630219]
68. Davis RB, Curtis CD, Griffin CT. BRG1 promotes COUP-TFII expression and venous specification during embryonic vascular development. Development. 2013; 140(6):1272–1281. [PubMed: 23406903]
69. Lizama CO, Hawkins JS, Schmitt CE, et al. Repression of arterial genes in hemogenic endothelium is sufficient for haematopoietic fate acquisition. Nat Commun. 2015; 6:7739. [PubMed: 26204127]
70. Yoshimoto M, Porayette P, Glosson NL, et al. Autonomous murine T-cell progenitor production in the extra-embryonic yolk sac before HSC emergence. Blood. 2012; 119(24):5706–5714. [PubMed: 22431573]
71. Böiers C, Carrelha J, Lutteropp M, et al. Lymphomyeloid Contribution of an Immune-Restricted Progenitor Emerging Prior to Definitive Hematopoietic Stem Cells. Cell Stem Cell. 2013; 13(5): 535–548. [PubMed: 24054998]
72. Lucitti JL, Jones EAV, Huang C, et al. Vascular remodeling of the mouse yolk sac requires hemodynamic force. Development. 2007; 134(18):3317–3326. [PubMed: 17720695]
73. Jones EAV, Baron MH, Fraser SE, et al. Measuring hemodynamic changes during mammalian development. Am J Physiol - Heart Circ Physiol. 2004; 287(4):H1561–H1569. [PubMed: 15155254]
74. Nakano H, Liu X, Arshi A, et al. Haemogenic endocardium contributes to transient definitive haematopoiesis. Nat Commun. 2013; 4:1564. [PubMed: 23463007]
75. Gordon-Keylock S, Sobiesiak M, Rybtsov S, et al. Mouse extraembryonic arterial vessels harbor precursors capable of maturing into definitive HSCs. Blood. 2013; 122(14):2338–2345. [PubMed: 23863896]
76. Chanda B, Ditadi A, Iscove NN, et al. Retinoic Acid Signaling Is Essential for Embryonic Hematopoietic Stem Cell Development. Cell. 2013; 155(1):215–227. [PubMed: 24074870]
77. Corada M, Nyqvist D, Orsenigo F, et al. The Wnt/β-Catenin Pathway Modulates Vascular Remodeling and Specification by Upregulating Dll4/Notch Signaling. Dev Cell. 2010; 18(6):938–949. [PubMed: 20627076]
78. Griffin CT, Curtis CD, Davis RB, et al. The chromatin-remodeling enzyme BRG1 modulates vascular Wnt signaling at two levels. Proc Natl Acad Sci USA. 2011; 108(6):2282–2287. [PubMed: 21262838]
79. Tober J, Yzaguirre AD, Piwarzyk E, et al. Distinct temporal requirements for Runx1 in hematopoietic progenitors and stem cells. Development. 2013; 140(18):3765–776. [PubMed: 23924635]
80. Huber TL, Kouskoff V, Joerg Fehling H, et al. Haemangioblast commitment is initiated in the primitive streak of the mouse embryo. Nature. 2004; 432(7017):625–630. [PubMed: 15577911]
81. Ueno H, Weissman IL. Clonal analysis of mouse development reveals a polyclonal origin for yolk sac blood islands. Dev Cell. 2006; 11:519–533. [PubMed: 17011491]
82. Padrón-Barthe L, Temino S, Villa del Campo C, et al. Clonal analysis identifies hemogenic endothelium as the source of the blood-endothelial common lineage in the mouse embryo. Blood. 2014; 124(16):2523–2532. [PubMed: 25139355]
83. Udan RS, Vadakkan TJ, Dickinson ME. Dynamic responses of endothelial cells to changes in blood flow during vascular remodeling of the mouse yolk sac. Development. 2013; 140(19):4041–4050. [PubMed: 24004946]
84. Kumano K, Chiba S, Kunisato A, et al. Notch1 but Not Notch2 Is Essential for Generating Hematopoietic Stem Cells from Endothelial Cells. Immunity. 2003; 18(5):699–711. [PubMed: 12753746]

85. Hadland BK, Huppert SS, Kanungo J, et al. A requirement for Notch1 distinguishes 2 phases of definitive hematopoiesis during development. Blood. 2004; 104(10):3097–3105. [PubMed: 15251982]

86. Lawson ND, Scheer N, Pham VN, et al. Notch signaling is required for arterial-venous differentiation during embryonic vascular development. Development. 2001; 128(19):3675–3683. [PubMed: 11585794]

87. Choi E, Kraus MR-C, Lemaire LA, et al. Dual Lineage-Specific Expression of Sox17 During Mouse Embryogenesis: Lineage-Specific Expression of Sox17. STEM CELLS. 2012; 30(10): 2297–2308. [PubMed: 22865702]

88. Cheng X, Huber TL, Chen VC, et al. Numb mediates the interaction between Wnt and Notch to modulate primitive erythropoietic specification from the hemangioblast. Development. 2008; 135(20):3447–3458. [PubMed: 18799543]

Significance Statement

While hematopoietic stem cell emergence from aortic endothelium has been extensively studied, the spatiotemporal location and regulation of yolk sac-derived hemogenic endothelium has remained largely undefined. Our studies capture morphological intermediates of the endothelial-to-hematopoietic transition of the first definitive hematopoietic progenitors in the murine yolk sac over developmental time. Interestingly, the emergence of erythro-myeloid progenitors is not restricted to arterial endothelium, nor is it dependent on blood flow, but is positively regulated by canonical Wnt signaling. Thus, hemogenic endothelium is more heterogeneous in location and hematopoietic output than previously recognized, and may help guide the derivation of definitive hematopoietic progenitors from pluripotent stem cells.

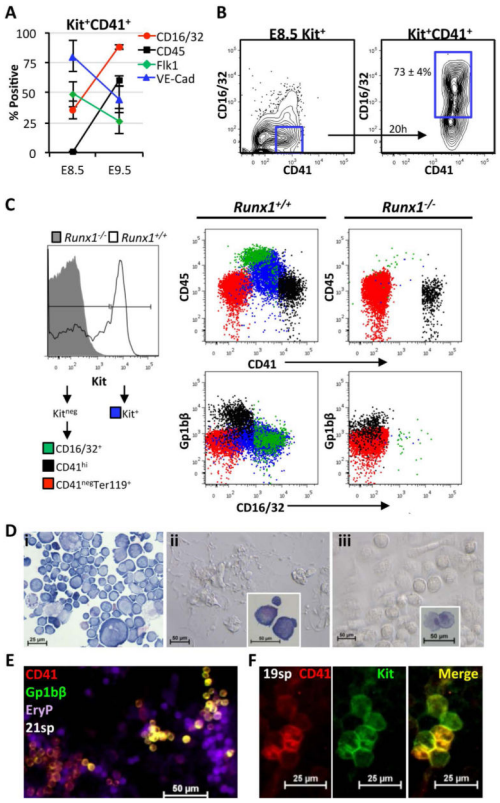

Figure 1. Emerging Kit^{+} EMPs progress from an endothelial to hematopoietic immunophenotype in a Runx1-dependent manner

A. The majority of E8.5 Kit^{+}CD41^{+} EMPs are negative for CD16/32 and CD45, and express endothelial markers Flk1 and VE-Cadherin. By E9.5, a higher proportion of the Kit^{+}CD41^{+} population expresses hematopoietic markers, with reduced endothelial marker expression. **B.** A significant portion of isolated E8.5 Kit^{+}CD41^{+}CD16/32^{neg} cells upregulate CD16/32 after 16–20 hours of *in vitro* culture. Plots from one representative experiment are shown; population percentages are the average of 3 experiments +/− SEM. **C.** Kit^{+} cells (blue) arise in *Runx1*$^{+/+}$ yolk sacs, but very few Kit^{+} events are detected in *Runx1*$^{-/-}$ yolk sacs. Kit^{neg} populations of immunophenotypic megakaryocytes (Kit^{neg}CD41^{hi}Gp1bβ^{+}, black) and macrophages (Kit^{neg}CD16/32^{+}CD45^{hi}, green), remain in *Runx1*$^{-/-}$ yolk sacs, albeit with significant depletion of immunophenotypic macrophages. Plots represent combined flow cytometric data from 4 E10.5 *Runx1*$^{+/+}$ yolk sacs and 4 E10.5 *Runx1*$^{-/-}$ yolk sacs. **D.** Culture of sorted E9.5 and E10.5 wildtype hematopoietic populations confirm EMP progeny (i, Kit^{+}CD41^{+}CD16/32^{+}), megakaryocyte potential (ii, Kit^{neg}CD41^{+}Gp1bβ^{+}), and macrophage potential (iii, Kit^{neg}CD16/32^{+}CD45^{+}). Images are of culture dishes (ii, iii) or Wright-Giemsa stained cytospins of cultures (i; ii and iii insets). n=2 pooled litters of yolk sacs. **E.** Immunohistochemical staining for CD41 demonstrates a significant overlap with Gp1bβ^{+}CD41^{hi} megakaryocytes in the E9.5 yolk sac, in addition to clusters of putative CD41^{+}Gp1bβ^{neg} EMPs. EryP, primitive erythroblast autofluorescence. n=3 yolk sacs. **F.** Kit^{+} cluster cells are CD41^{+} and CD41$^{lo/neg}$ by immunohistochemistry. n=5 yolk sacs.

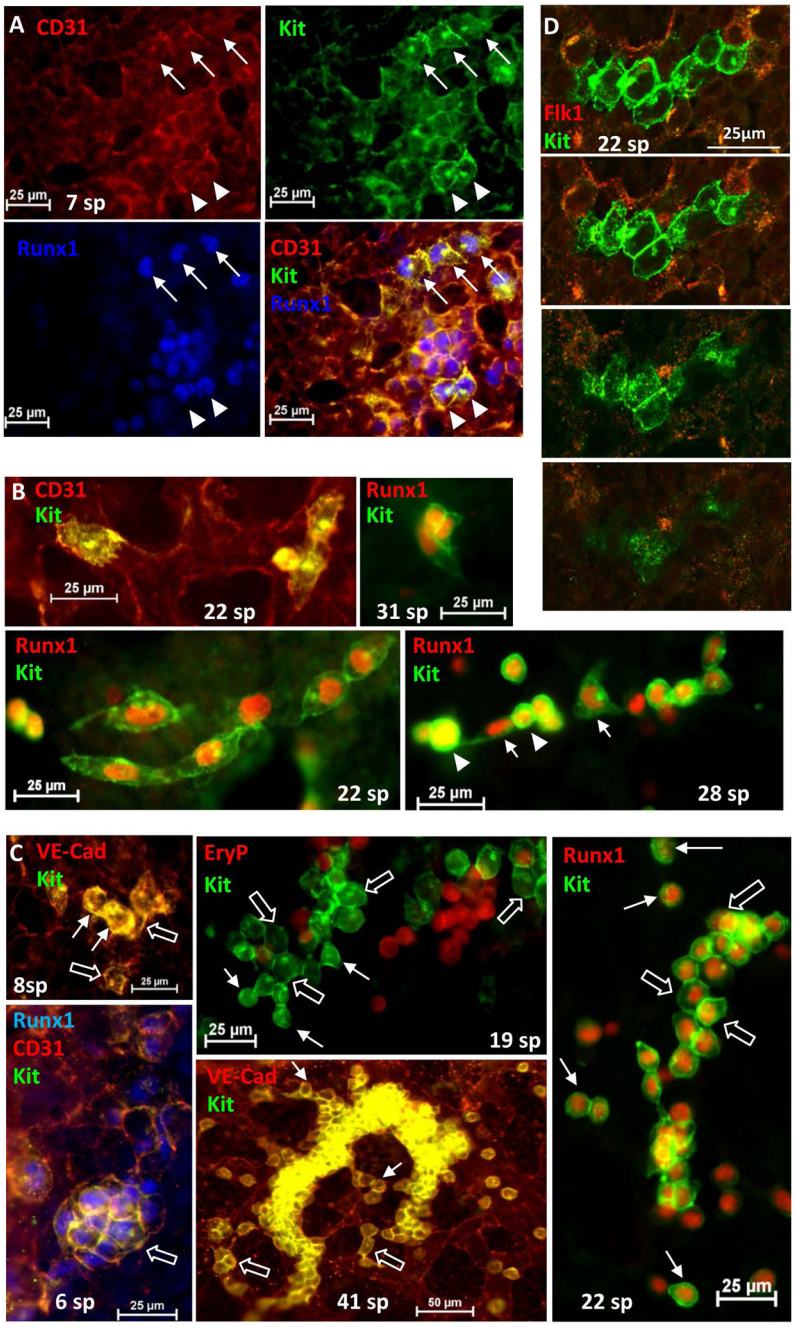

Figure 2. EMPs emerge from morphologic hemogenic endothelium between E8.5-E11

Immunohistochemistry at the stages indicated with indicated markers. **A.** Flattened and rounded Kit$^+$ cells are detected at E8.5. Arrows indicate flattened hemogenic endothelial cells; arrowheads indicate rounded hematopoietic cells. **B.** Examples of flattened hemogenic endothelial cells at E9.5-E10. Bottom right has both Runx1$^+$Kit$^+$ rounded cells (arrowheads) and Runx1$^+$Kit^{lo} flattened cells (arrows). **C.** Examples of polygonal Kit$^+$ clusters (open arrows) and rounded Kit$^+$ cells (closed arrows) at E8.5 (6, 8 somite pairs (sp)), E9.5 (19, 22 sp), and E11 (41 sp). **D (top right).** Confocal Z-stacks through a polygonal Kit$^+$ cluster at E9.5 indicates Kit$^+$ cells are in the same plane of focus as the endothelium.

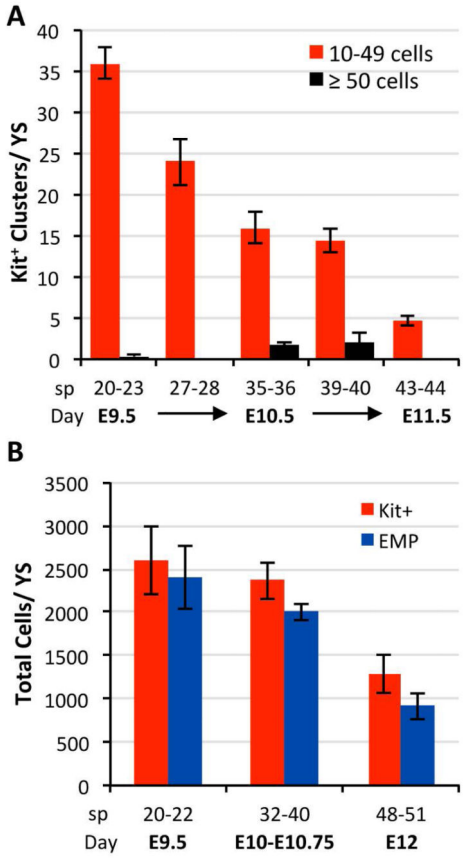

Figure 3. EMPs continually emerge over a broad developmental time and remain in the yolk sac circulation as late as E12

A. Quantification of immunohistochemical Kit$^+$ clusters in the yolk sac (YS) over developmental time. n=3 for all timepoints except 39–40sp (E11) (n=4). Error bars indicate SEM. Significance was determined (10–49 cells; $P = 4.81\text{x } 10^{-6}$) by one-way Analysis of Variance. All means (10–49 cells) are significantly different from one another ($P < 0.05$, Tukey-Kramer post-test) except: 27–28sp and 35–36sp; 35–36sp and 39–40sp. **B.** Flow cytometry indicates that robust numbers of Kit$^+$ cells, many of which are Kit$^+$CD41$^+$CD16/32$^+$ EMPs, remain in the yolk sac circulation through E11, and begin to decline by E12. n=3 20–22sp, n=5 32–40sp, n=4 48–51sp. Error bars indicate SEM. Significant differences within each fraction were determined by one-way Analysis of Variance: $P = 0.012$ (Kit$^+$), $P = 0.001$ (EMP). All means are significantly different from one another ($P < 0.05$, Tukey-Kramer post-test) except 20–22sp and 32–40sp (both Kit$^+$ and EMP).

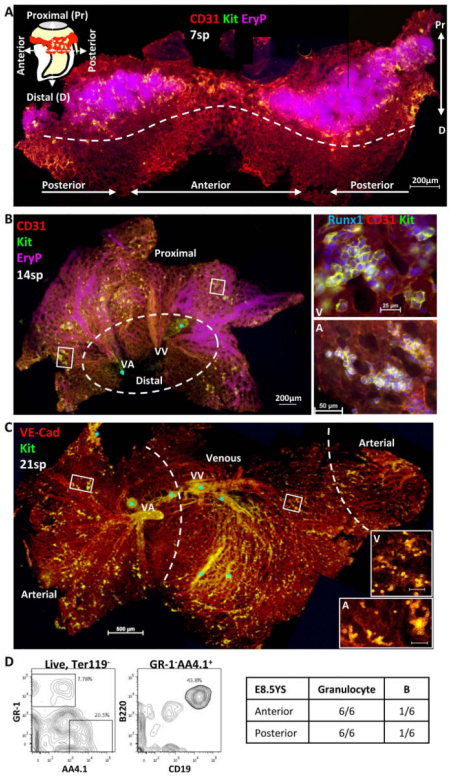

Figure 4. EMPs emerge along a proximal-distal gradient without anterior/posterior or arterial/venous preference

A–C. Immunohistochemistry at the stages indicated with indicated markers. **A**. Schematic represents an intact E8.5 embryo for clarity of anatomical locations within the flat-mounted yolk sac. EMP clusters are interspersed within the anterior and posterior regions of the blood island region of the proximal yolk sac (above the dotted line), where the primitive erythroblasts (EryP; purple) are also located. See Fig. S2 for images of each separate stain. **B.** By 14sp (E8.75), EryPs start to appear in the distal portion of the yolk sac (inside dotted circle), while EMP clusters remain in the proximal yolk sac (outside dotted circle). Blue asterisks in both B and C indicate background artifact; see Fig. S2. Boxed regions indicate clusters in venous (V) and arterial (A) regions (B, right; C, insets). **C.** At 21sp (E9.5), EMP clusters reside in both the arterial and venous regions of the yolk sac (approximated by dotted lines). Scale bar of insets: 50μm. The vitelline artery was identified based on distinct branching morphology[68], which was corroborated both with Sox17 labeling (see Fig. S3), and by identification of $Kit^{+}Runx1^{+}$ clusters in extensions of the artery (not shown). **D.** Anterior and posterior regions of the E8.5 yolk sac each produce GR-1^{+} granulocytes. B-lymphocyte potential is also evident. Flow cytometric analysis of one anterior culture shown at day 12.

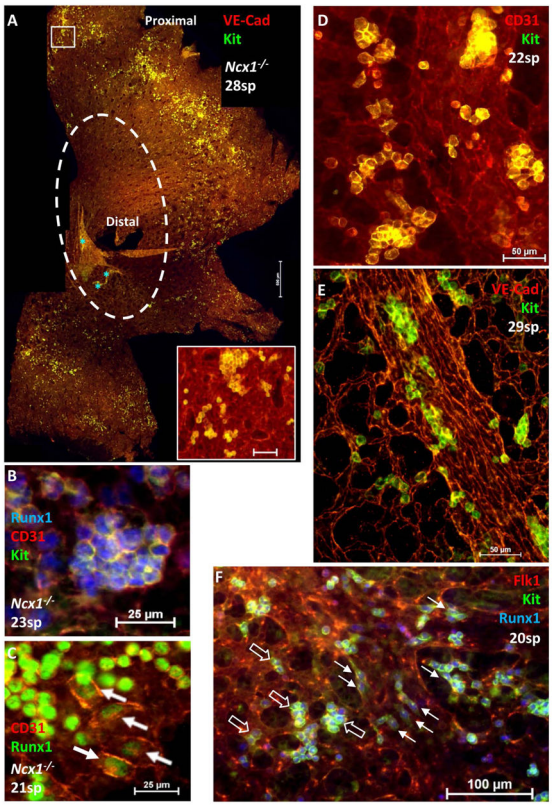

Figure 5. The endothelial-to-hematopoietic transition occurs without circulation, and in larger and smaller vessels after vascular remodeling

A. EMP clusters in the *Ncx1*$^{-/-}$ yolk sac are localized to the proximal region. Blue asterisks indicate background artifact from folded tissue. Scale bar: 500μm; inset: 50μm. **B–C.** Examples of polygonal Kit^{+}CD31^{+}Runx1^{+} clusters (B) and flattened Runx1^{+} hemogenic endothelial cells (C, arrows) in E9.5 *Ncx1*$^{-/-}$ yolk sacs. 3 *Ncx1*$^{-/-}$ yolk sacs were analyzed. **D–F.** At E9.5-10, flattened and polygonal Kit^{+} cells are present in larger remodeled vessels and the vascular plexus. (F) Flattened Kit^{lo}Runx1^{+} cells are denoted by closed arrows, polygonal cells by open arrows.

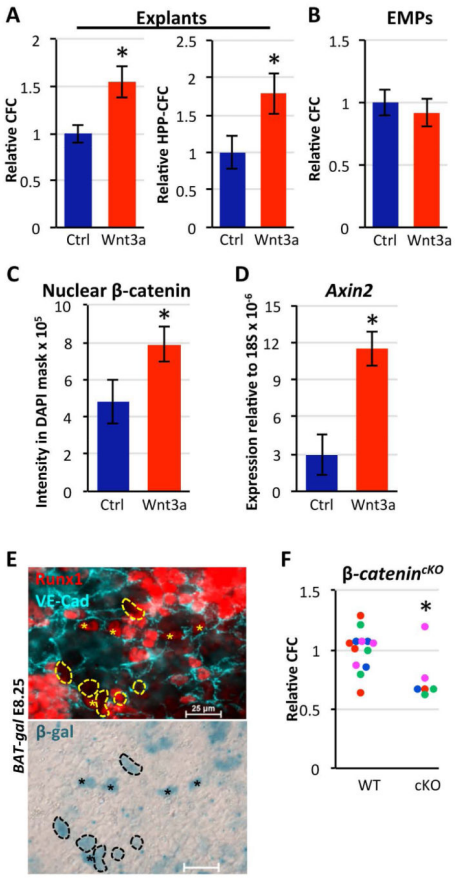

Figure 6. Canonical Wnt signaling regulates EMP production *in vitro* and *in vivo*

A. Increased production of CFCs and HPP-CFCs in explanted E8.5 yolk sacs with Wnt3a treatment. (Left) Methylcellulose culture (CFCs) of 6–7sp yolk sacs. n=10. (Right) HPP-CFC of 7–9sp yolk sacs (n=7 controls (Ctrl), n=8 Wnt3a treated). Error bars indicate SEM. **P* <0.05, 2-tailed student's t-test. **B.** No changes in CFC activity were observed with Wnt3a treatment of sorted E9.5-E10 $Kit^+CD41^+CD16/32^+$ EMPs for 24 hours. n=5, error bars indicate SEM. **C.** Wnt3a treatment of E9.5 dissociated yolk sacs for 2 hours increased β-catenin staining intensity in the nuclear region of $Kit^+VEC/AA4.1^+CD16/32^{neg}$ cells. n=3, error bars indicate SEM. **P* <0.01, 1-tailed student's t-test. **D.** Treatment of sorted $VEC/AA4.1^+CD16/32^{neg}$ cells with Wnt3a for 5 hours increased expression of β-catenin target gene Axin2. n=3. **P* <0.05, 1-tailed student's t-test. **E.** Immunohistochemistry and β-galactosidase (β-gal) staining of E8.25 *BAT-gal* yolk sac reveals a rare subset of $VEC^+Runx1^+β\text{-}gal^+$ putative hemogenic endothelium (asterisks). 1 example of 4 yolk sacs with $VEC^+Runx1^+β\text{-}gal^+$ staining is shown. $Runx1^{neg}β\text{-}gal^+$ cells (dotted lines) are also present. The majority of $Runx1^+$ cells are $β\text{-}gal^{neg}$. For whole yolk sac images, see Fig. S4B. **F.** E9.5-E10.5 *Cdh5-Cre; Ctnnb1*$^{fl/fl}$ yolk sacs (cKO) have reduced CFCs compared with yolk sacs of *Cdh5-Cre*^{neg} littermates. Colors of data points represent separate litters of embryos (n=4 litters). **P* =0.01, 1-tailed student's t-test.

A

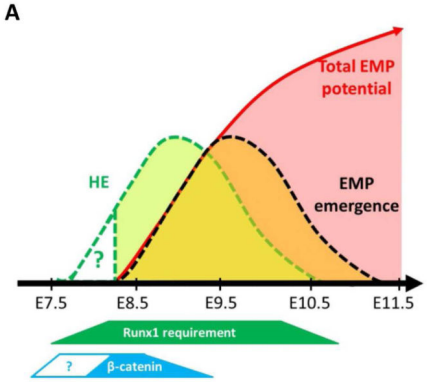

B

Requirement or Timing	EMPs	HSCs	Refs
Onset (Murine)	E8.25-E11	E10.5-E12.5	[1, 6, 27]
Location (Murine)	Yolk sac	Aorta UA VA	[1, 2, 39]
Runx1	Yes	Yes	[3, 4]
HE	Yes	Yes	[7-10]
Arterial/Venous	Plexus/Both	Arterial	See location
Circulation/NO	No	Yes	[21, 22]
Notch1	No	Yes	[84, 85]
Wnt/β-catenin	Yes	Yes	[25, 26]

Figure 7. Summary of EMP specification in the murine yolk sac and comparison with HSC specification

A. Temporal model of yolk sac-derived definitive hematopoiesis. Hematopoietic potential is initiated as a wave of EMP colony-forming activity over developmental time (red arrow with shaded area)[27]. Analysis of hemogenic endothelial-derived Kit^+ cluster numbers indicates that EMPs cease to emerge in the yolk sac after E11.5 (black dotted line, orange shaded area). This wave of hematopoietic emergence is preceded by the appearance of flattened hemogenic endothelium (HE; green dotted line) from E8.5 through as late as E10.5-11, as determined in Figure 2. The observed formation of hemogenic endothelium correlates well with the reported requirement of Runx1 in mediating EMP formation through E10.5 (green trapezoid)[79]. Note that presence of hemogenic endothelium at early developmental stages (green triangle) is approximated and remains unknown. Endogenous canonical Wnt signaling in the yolk sac is robust at early stages (blue trapezoid), and increases EMP production from hemogenic endothelium at E8.5 (green dotted line) *ex vivo*, as determined in Figure 6. Together, these kinetics suggest that canonical Wnt signaling has an early role in regulating hematopoietic potential from hemogenic endothelium. **B**. Comparison of the timing of and requirements for EMP and HSC emergence. UA, umbilical artery; VA, vitelline artery; HE, hemogenic endothelium, NO; nitric oxide.